Journal of Power Sources 422 (2019) 42–48

Contents lists available at ScienceDirect

Journal of Power Sources

journal homepage: www.elsevier.com/locate/jpowsour

Sodium insertion in high pressure β-V_2O_5: A new high capacity cathode material for sodium ion batteries

Rafael Córdoba[a], Alois Kuhn[a], Juan Carlos Pérez-Flores[a,1], Emilio Morán[b], José Manuel Gallardo-Amores[c], Flaviano García-Alvarado[a,*]

[a] Universidad CEU San Pablo, Facultad de Farmacia, Departamento de Química y Bioquímica, Urbanización Montepríncipe, 28668, Boadilla del Monte, Madrid, Spain
[b] Universidad Complutense, Facultad de Ciencias Químicas, Departamento de Química Inorgánica, Ciudad Universitaria s/n, 28040, Madrid, Spain
[c] Universidad Complutense, Facultad de Ciencias Químicas, Laboratorio Complutense de Altas Presiones, Ciudad Universitaria s/n, 28040, Madrid, Spain

HIGHLIGHTS

- High pressure β-V_2O_5 inserts 1 Na/formula unit at high voltage.
- Insertion of 1 sodium in β-V_2O_5 proceeds through 5 solid solutions.
- β-V_2O_5 delivers 147 mAh/g upon sodium insertion in the 3.6–2.0 V range.
- β-V_2O_5 unveiled as a promising cathode material for sodium ion batteries.
- An irreversible phase transformation does not affect further cyclability.

GRAPHICAL ABSTRACT

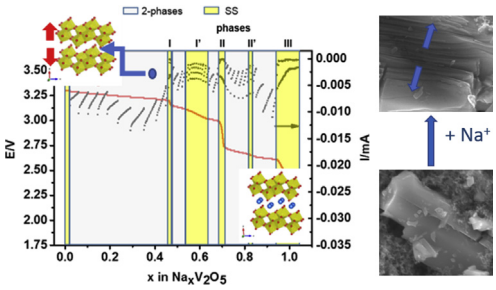

ARTICLE INFO

Keywords:
Vanadium oxide
Sodium insertion
Battery material
Cathode
Ex situ XRD

ABSTRACT

β-V_2O_5, obtained by a high-temperature high-pressure method, exhibits a layered structure that favours the insertion of Na^+. In this work, we report the electrochemical insertion of sodium in high pressure β-V_2O_5 and its performance as cathode material for sodium-ion batteries. The material shows a first discharge capacity of 132 mAh g^{-1} in the 3.6–2.0 V range at a C/20 current density and a maximum capacity of 147 mAh g^{-1} under equilibrium conditions, corresponding to the insertion of 1 Na^+ ion per formula unit. The β-V_2O_5//Na cell delivers a specific energy as high as 370–410 Wh kg^{-1}. The amount of inserted sodium points to the reduction of 50% of the available V^{5+} ions. After 20 cycles, the discharge capacity retains 86% of the initial capacity. Concerning the reaction mechanism of high pressure β-V_2O_5 upon sodium insertion/de-insertion, several phase transitions are inferred from the voltage-composition profile. Ex situ XRD reveals the appearance of several $Na_xV_2O_5$ phases in the $0 \leq x \leq 1$ compositional range, which are closely related with the non-sodiated high pressure β-V_2O_5 structure. An irreversible structural transformation occurs during the very first inserted sodium, at the beginning of the first discharge, and the original high pressure β-V_2O_5 structure is not recovered upon full Na^+ extraction. Electrochemical performances are outstanding though.

1. Introduction

The success of lithium-ion batteries in the electronic market has triggered their use in electrical vehicles and even large-scale energy storage. To alleviate the scarcity of lithium resources, this latter application may be better addressed by using sodium batteries. These

* Corresponding author.
E-mail address: flaga@ceu.es (F. García-Alvarado).
[1] Present Address: Instituto de Investigación de Energías Renovables, Universidad de Castilla-La Mancha, 02006 Albacete, Spain.

https://doi.org/10.1016/j.jpowsour.2019.03.018
Received 4 December 2018; Received in revised form 21 February 2019; Accepted 7 March 2019
Available online 16 March 2019
0378-7753/

batteries, though developing less specific capacity with present available sodium insertion hosts [1], have the advantage of lower cost due to the high abundance of sodium. Thus, a great effort is now being made to unveil new materials able to intercalate large amount of sodium at either high or low potential. Taking into account the available materials for the cathode, capacity seems to be limited to 150 mAh g^{-1} ($NaFePO_4$, Na_2FePO_4F, etc. [2]) and, as in the case of lithium-ion battery materials, the investigation of possible two-electron systems is relevant. Among V-compounds able to provide two electron transfer upon lithium insertion, Li_2VO_2F with a disordered cubic rock-salt structure (space group Fm-3m) [3] has a theoretical capacity of 462 mAh g^{-1}, which significantly exceeds that of the conventional $LiCoO_2$ and $LiFePO_4$ cathode materials. VO_2F with a rhombohedral R-3c structure, obtained using a high-temperature high-pressure solid-state reaction delivers 250 mAh g^{-1} above 2.15 V. A higher capacity can be even reached at the expense of a lower voltage output though [4]. Motivated by the high capacity exhibited by this oxyfluoride a more easily scalable preparation method based on high-energy ball-milling was developed shortly after [5]. Thus, even though high-pressure materials seem to be far from large-scale application, unveiling their properties may trigger new advances in synthesis to make them easily available.

The high capacity and cycling stability [6] of ambient pressure α-V_2O_5 makes it an interesting candidate as cathode for lithium-ion batteries. It should be noted that its high pressure form β-V_2O_5 (HP-β-V_2O_5 hereafter) [7] has also been proposed as host for Li-ion batteries [8], and 2 Li^+/formula unit are reversibly intercalated upon discharge to 1 V vs. Li^+/Li. A remarkable capacity of 250 mAh g^{-1} is observed after 80 cycles [8]. The lithium insertion mechanism, however, seems to be very intriguing, since at least six different $Li_xV_2O_5$ phases were detected.

Even though most of the high pressure polymorphs present a significant decrease of cell volume (denser structures) and higher coordination numbers [9,10] than the corresponding ambient pressure forms, in some of them, such as HP-β-V_2O_5, volume reduction is not very high [7,11] and are therefore interesting as cathode materials for batteries. In contrast, the high-pressure form [11] of olivine $LiFePO_4$ is electrochemically inactive. In HP-β-V_2O_5 each vanadium atom is coordinated to six oxygen atoms, making up distorted [V−O_6] octahedra [7]. Specifically, the structure consists of quadruple units of [V−O_6] octahedra, which share edges; and these units are arranged in layers (Fig. S1 of Supporting Information).

In this work, we investigate the suitability of HP-β-V_2O_5 for Na^+ ion insertion reaction in the high voltage range (above 2 V) in view of its use as the cathode in Na-ion batteries. HP-β-V_2O_5 with a layered structure is obtained by a high-temperature high-pressure method [7]. Although at a first thought, a compound obtained by high-pressure synthesis may not seem to be viable for being used as a battery electrode (due to the predicted lack of vacancies or channels for cation diffusion), the truth is that the layered structure of HP-β-V_2O_5 has been shown to favour the insertion of Li^+ [8]. In this report we show that up to 1 Na^+ ion/formula unit can be intercalated, developing a significant capacity of 147 mAh g^{-1}. Furthermore, the structural changes upon sodium insertion in HP-β-V_2O_5 have been monitored with ex situ XRD. Interestingly, ambient pressure α-V_2O_5 is known to be electrochemically susceptible to Na^+ insertion, but only through special morphologies, like nanoparticles [12,13], nanocomposites [14] or xerogels [15]. It is worth saying that commercial (ambient pressure) vanadium pentoxide exhibits rather poor electrochemical Na^+ insertion properties, as will be shown in the Results and Discussion section. Interestingly, ab initio studies have shown that calculated ion diffusion barrier of sodium in α-V_2O_5 is much higher than the one calculated for sodium in HP-β-V_2O_5 [16]. Thus, performances of HP-β-V_2O_5 as cathode material for sodium batteries are expected to be much better.

It is important to note that there is some contradiction in the literature regarding the proper nomenclature of β-V_2O_5. Concerning crystal chemistry, Volkov et al. [17] initially indexed the X-ray diffraction pattern of β-V_2O_5 (ICDD PDF 4591074) with a very large tetragonal cell with a = 14.259 Å, *c* = 12.576 Å (V = 2557 $Å^3$). Later, Filonenko et al. [7] solved the crystal structure of β-V_2O_5 by X-ray and neutron powder diffraction. It crystallizes monoclinic, space group $P2_1/m$, with a = 7.1140(2) Å, b = 3.5718(1) Å, c = 6.2846(2) Å and β = 90.069(3)° (V = 160 $Å^3$). Other authors [18–21] claim to have prepared "β-V_2O_5" under different synthesis conditions. However, the quality of crystallographic data reported in these papers is rather poor, and the indexation of the X-ray patterns, based on a few diffraction maxima, likely due to preferred orientation effect, does not match either with the initial (wrong) unit cell reported by Volkov et al. [17] Therefore, the V_2O_5 samples reported by these authors are much likely different forms of vanadium pentoxide.

We must note that upon sodium intercalation in HP-β-V_2O_5 the phases formed have the nominal composition $Na_xV_2O_5$, and their structures obtained through topotactic reaction, relate to HP-β-V_2O_5 (S.G: P 2_1/m, layered) [22]. However, the sodium bronze β-$Na_{0.33}V_2O_5$ (S.G: *C2/m*, tunnel structure) which exhibit a quite different structure and is also able to intercalate additional sodium [13], produces β-$Na_{0.33+x}V_2O_5$ phases which are related to the bronze structure. Therefore, both sodiated compounds would have different structures.

2. Experimental

Synthesis of HP-β-V_2O_5 was carried out by treating previously dried α-V_2O_5 (Aldrich, 99.9%) in a belt-type press at 40 kbar and 800 °C for 30 min [7].

X-ray diffraction measurements were performed by means of a Bruker D8 high-resolution diffractometer equipped with a solid-state position sensitive rapid LynxEye® detector (PSD), using dichromatic CuKα radiation (λ = 1.5406 Å, 1.54439 Å).

Morphological characterization of pristine HP-β-V_2O_5, a pristine electrode and an electrode after cycling was carried out by means of Scanning Electron Microscopy (SEM) using a JEOL JSM-6400 microscope.

Electrochemical experiments were performed in CR2032 coin cells assembled in argon atmosphere. Sodium metal was used as the negative electrode and stacked with a glass fibre paper separator and a positive electrode all immersed in a 1 M $NaClO_4$ 1:1 solution of ethylene carbonate (EC) and propylene carbonate (PC) as the electrolyte. Preliminary electrochemical characterization was carried out on 8 mm diameter pellets pressed from a HP-β-V_2O_5, Super P Timcal carbon and PVDF composite in an 85:10:5 wt ratio, respectively. For longer cycling studies and C-rate performances, a slurry containing HP-β-V_2O_5, Super P Timcal carbon and PVDF in an 80:10:10 wt ratio was cast onto aluminium foil from which electrode disks with 12 mm diameter were cut. For ex situ XRD studies, positive electrodes with 10 mm diameter were discharged in Swagelok™ type cells against sodium metal until the desired Na compositions were reached. Galvanostatic discharge-charge experiments were carried out at different C/n rates, i.e. a current to provide insertion of 1 Na in n h. The voltage at which processes take place were determined by cyclic voltammetry measurements which were run at 10 mV/10 min rate in the 3.6–2.0 V potential range. Near equilibrium experiments were performed in the 3.6–1.7 V voltage range using the galvanostatic intermittent titration technique (GITT) to estimate the composition of phases between x = 0 and x = 1. A current of 82.5 μA was applied for 30 min to reach a 0.025 incremental change of sodium content. The cell was allowed to relax afterwards for 4 h. Potentiostatic intermittent titration technique (PITT) experiments were run to analyse the nature of the insertion reactions. A cell was discharged at 10 mV steps every 8 h in the 3.5–2.0 V voltage range.

Impedance spectroscopy was used to analyse the change in the charge transfer process upon cycling. Typical experiments were performed at open circuit voltage condition in a two-electrode cell before and after cycling. The measurements were carried out at room temperature using a VMP3 battery tester with an Electrochemical

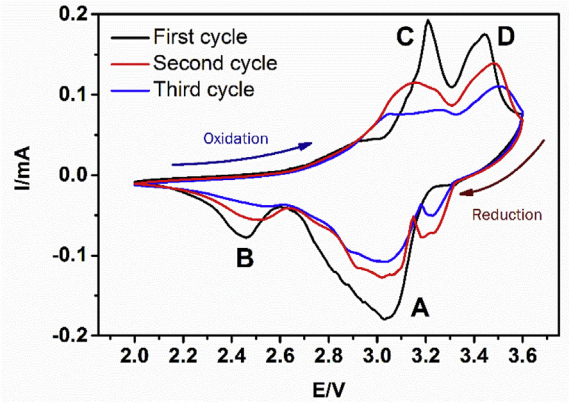

Fig. 1. Voltammograms at a 10mV/10min step rate in the 3.6–2.0 V range corresponding to reduction-oxidation cycles of HP-β-V_2O_5.

Impedance Spectroscopy channel. A sinusoidal potential perturbation of 10 mV was applied while measuring impedance variation in the frequency range from 3×10^5 Hz–0.1 Hz.

3. Results and discussion

The high-pressure synthesis produced a reddish-brown powder that was determined to be HP-β-V_2O_5 according to the X-ray powder diffraction pattern (Fig. S2 of Supporting Information). Refined lattice parameters fully agree with those previously reported [7]. Experimental conditions and refined lattice parameters are given in Table S1 of Supporting Information, whereas main structural parameters of the Rietveld refinement are listed in Table S2 of Supporting Information.

Fig. 1 shows three consecutive voltammograms obtained at a 10 mV/10 min scan rate in the 3.6–2.0 V range vs Na^+/Na. The first reduction wave shows two processes, labelled with A and B and centred at 3.1 and 2.5 V, corresponding to a two-step reduction of V^{5+} to V^{4+}. However, the peak A seems to involve at least two different processes and a shoulder on the low voltage side is inferred from the pronounced asymmetry of the peak. Two intense peaks, labelled with C and D, appear at 3.15 and 3.4 V in the oxidation wave. Their profiles and peak separation, however, do not point to a full correspondence with the peaks A and B observed in the first reductive wave. Furthermore, the second reduction wave reveals significant differences with respect to the first reduction wave. This may point to a (structural) change in HP-β-V_2O_5 during the first reduction, but after which reversible oxidation and reduction continues, as it can be deduced from the similarities of second and third reduction-oxidation waves.

Fig. 2a shows the galvanostatic discharge-charge cycles at C/20 current rate of HP-β-V_2O_5 obtained from a slurry cast onto aluminium foil. Ca. 0.9 Na^+/f.u. (132 mAh g^{-1}) are intercalated in the first discharge which are fully deintercalated upon charge (Fig. 2a). The second and third discharge cycles show a quite similar profile, however the loss of capacity is evident. Capacity slightly decreases in the first few cycles (Fig. 2b), as usually found for composite electrodes. For instance the same effect has been observed for nanowires of the bronze β-$Na_{0.33}V_2O_5$ [13]. Further cycling of HP-β-V_2O_5 at C/20 and C/10 is accompanied by an increase of capacity to stable 120 mAh g^{-1} and 80 mAh g^{-1}, respectively (Fig. 2b). We ascribe this phenomenon to electrochemical milling that may reduce kinetic limitations and polarization therefore. However, this effect is not clearly observed at higher current rates (C/5) for which decrease of polarization due to electrochemical milling may be negligible compared to polarization due to high current.

Interestingly, α-V_2O_5 shows a very different electrochemical behaviour [12,23–25]. For comparison, an electrode bearing (commercial) polycrystalline α-V_2O_5 has been ellaborated using the same procedure

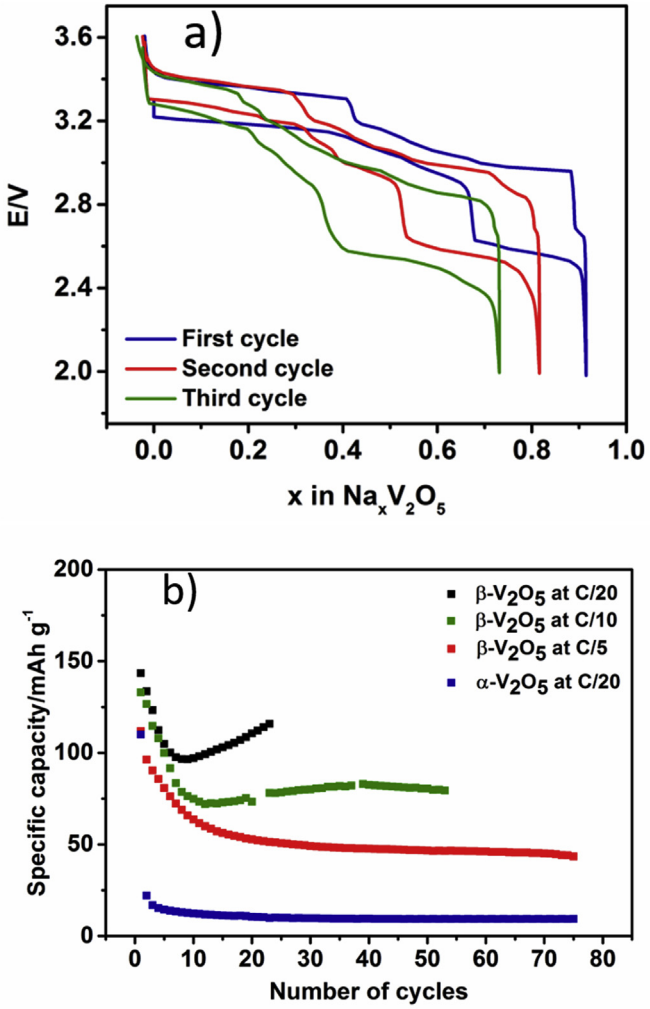

Fig. 2. First three discharge-charge cycles of HP-β-V_2O_5 in the 3.6–2.0 V range at a C/20 rate (a); evolution of specific capacity with number of cycles for HP-β-V_2O_5 at C/20, C/10 and C/5 and commercial polycrystalline α-V_2O_5 at C/20 (b).

as for HP-β-V_2O_5 and was then cycled at C/20 in the same voltage range as HP-β-V_2O_5.

α-V_2O_5 develops a first discharge capacity of 110 mAh g^{-1} (Fig. 2b), however severe capacity fading with complete loss of capacity is observed after a few cycles. Lee et al. [13] have recently shown that α-V_2O_5 nanowires exhibit better performance, however much lower than HP-β-V_2O_5. This demonstrates impressively the better electrochemical performance of HP-β-V_2O_5 able to deliver a maximum specific capacity of 147 Ah kg^{-1} and specific energy of 411 Wh kg^{-1}.

Kulish et al. have proposed, based on first principles calculations, that HP-β-V_2O_5 may be the most promising vanadium oxide cathode for Na-ion batteries due to a much improved diffusion kinetics and significant lower diffusion barriers when compared with α-V_2O_5 and other vanadium oxides [16].

The cycling performance of the HP-β-V_2O_5 electrode at different C rates is shown in Fig. 3. At low C rates, good performance of HP-β-V_2O_5 is observed with more than 50% capacity at C/5. However, it cannot stand significant capacity for 1C. Nevertheless, taking into consideration that capacity is greatly recovered when cycling at C/20, this material is worth being further investigated as a promising cathode material for sodium-ion batteries. Electrochemical experiments reveal an important kinetic limitation of this electrode. Note that the material has been used as prepared (large particle size). Fig. 4a shows a SEM image of a pristine electrode with the inset showing the powder used for its

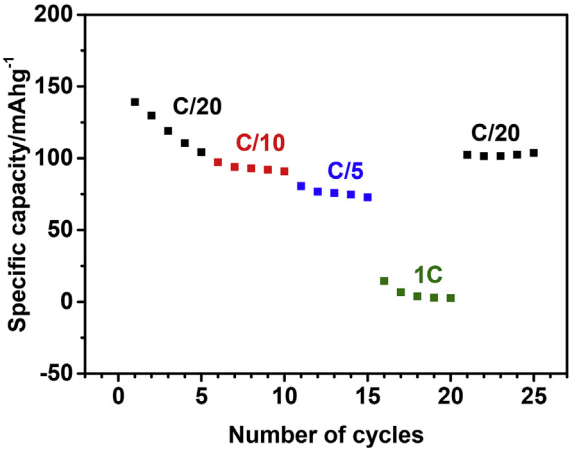

Fig. 3. Variation of specific capacity of a Na || HP-β-V_2O_5 cell at different C/n rates where n stands for the number of hours needed to insert 1 Na^+/V_2O_5.

fabrication. Well-defined prismatic microcrystals ranging from 1 to 10 μm can be seen in both the powder and the electrode. The "foam" surrounding the crystals in the electrode is the binder used to fabricate the electrode. The morphology of the as prepared HP-β-V_2O_5 is not likely optimum for intercalation reactions, but high-pressure synthesis route does not provide an easy way to obtain crystals having more appropriate morphologies to improve rate performance.

Fig. 4b shows a SEM image of an electrode cycled 150 times at C/5 rate

As most striking feature this image reveals that though big crystals in the micrometric scale are still present, these were partially cleaved (see regions marked with red arrows). Green circles indicate regions of binder and blue squares, glass fibres from silicon-based separator.

It is likely that a more extended cleavage of V_2O_5 crystals would be a way of improving rate performances of this new cathode material for sodium-ion batteries. On the other hand, new synthetic methods need to be developed to overcome kinetic limitations by tailoring morphology.

Impedance spectroscopy has been carried out to investigate the change of charge transfer resistance upon cycling. Nyquist plots of a fresh cell, after 4 and 188 cycles at C/5 are shown in Fig. S3 of the Supporting Information. At high and medium frequencies, depressed semicircles are followed by a straight line, except for the spectrum taken after 4 cycles. Spectra of a fresh electrode and an electrode after 38 cycles have been satisfactorily fitted to the equivalent circuit shown in the insets of Fig. S3 used by Lee at al [13]. for related compounds. R_s corresponds to low resistance of the electrolyte through the connecting pores of separator. A resistor R_f in parallel with a distributed element depending on frequency (CPE_f) describes the impedance of the sodium electrode and thin insulating layer that may be formed due to reaction with the electrolyte at different potential. Finally, a modified Randles-type circuit describes the resistance of the charge-transfer process (R_{ct}), the double layer capacity (C_{dl}) that due to the roughness of the electrode is replaced by a distributed element depending on frequency (CPE_{dl}), and the diffusion of sodium within particles is described with a Warburg element (W_s). For the spectrum taken after 4 cycles the Warburg element has been eliminated during the fitting, because the straight line was not clearly observed at low frequency due to dispersion of data. The value of the charge-transfer resistance (ca. 400 Ω) is very high for the pristine electrode, indicating a limited kinetics. The charge transfer of the electrode cycled four times decreases and results to be quite low (ca. 70 Ω) because of a non-reversible phase transition taking place after the very first sodium atoms inserted during the first discharge (see below). Finally, extended cycling produces an increase of charge transfer resistance (115 Ω) due to aging of the electrode and increase of surface resistance. However, charge-transfer remains much lower than in the case of fresh β-V_2O_5.

Fig. 5 shows the open circuit voltage of a Na|| HP-β-V_2O_5 cell discharged in the galvanostatic intermittent mode. The upper open circuit voltage region is characterized by a long plateau centred at 3.3 V that can be assigned to a two phase region. Between 3.2 and 3.1 V a voltage drop occurs in a narrow compositional range (region I) pointing to the existence of a narrow solid solution region. Between 3.1 and 2.9 V a pseudo-plateau is observed pointing to a biphasic region. This finding agrees with the fact that reduction peak A in the voltammogram (Fig. 1) seemed to consist of at least two different processes very close to each other. A third plateau is observed at ca. 2.60 V which separates two other narrow solid solution ranges (II and III) and corresponds to the reduction process labelled as peak B in Fig. 1. Taking into consideration results from the discharge curve shown in Fig. 5 and reduction wave in Fig. 1, the following compositional ranges can be proposed for HP-β-$Na_xV_2O_5$ single phases formed during the first reduction:

Phase I: x = 0.35–0.45

Phase II: x = 0.65–0.7

Phase III: x = 0.9–1.0

Formation of phase III corresponds to the maximum amount of sodium that can be intercalated in HP-β-V_2O_5 in this voltage range (1 Na ion/f.u.). The charge curve of the open circuit voltage experiment depicted in Fig. 5 also shows the same voltage characteristic as the discharge curve except for a less marked evidence of phase II formation.

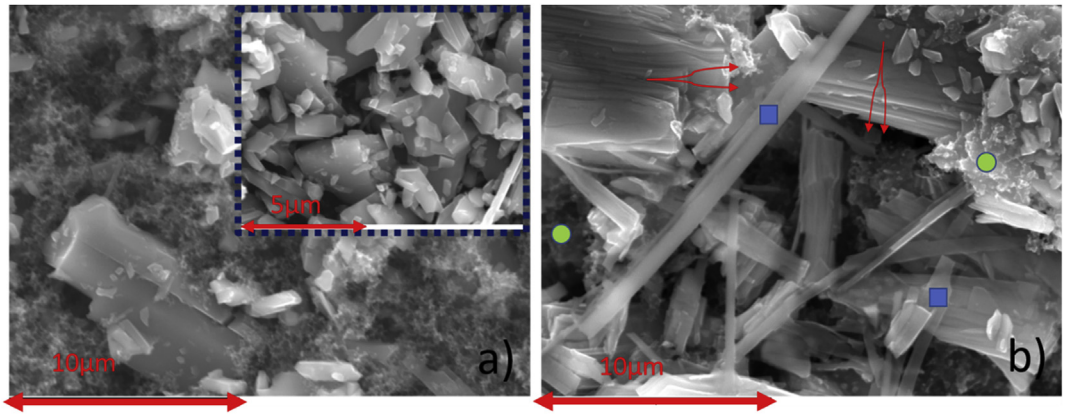

Fig. 4. SEM images of a composite electrode with HP-β-V_2O_5 as the active material before cycling (a) and after 150 cycles at C/5 rate (b). Green circles: binder; blue squares: glass fibre from separator. The inset shows the pristine powder of HP-β-V_2O_5 used for electrode fabrication. (For interpretation of the references to colour in this figure legend, the reader is referred to the Web version of this article.)

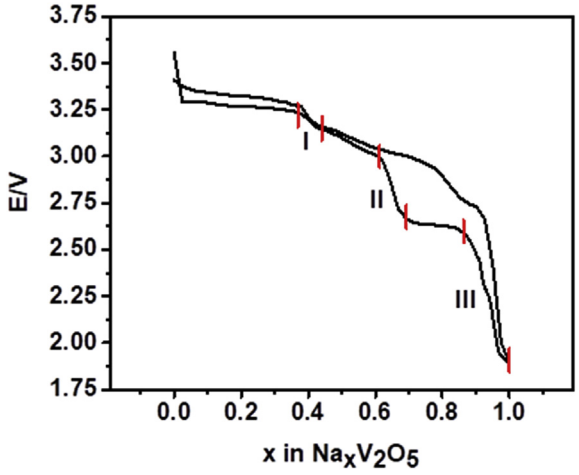

Fig. 5. Open circuit voltage of a Na|| HP-β-V_2O_5 cell discharged in the galvanostatic intermittent mode in the 3.6–1.7 V range at a current equivalent to a C/20 discharge in continuous mode for 0.5 h. Cell was kept at open circuit for 4 h between current intervals.

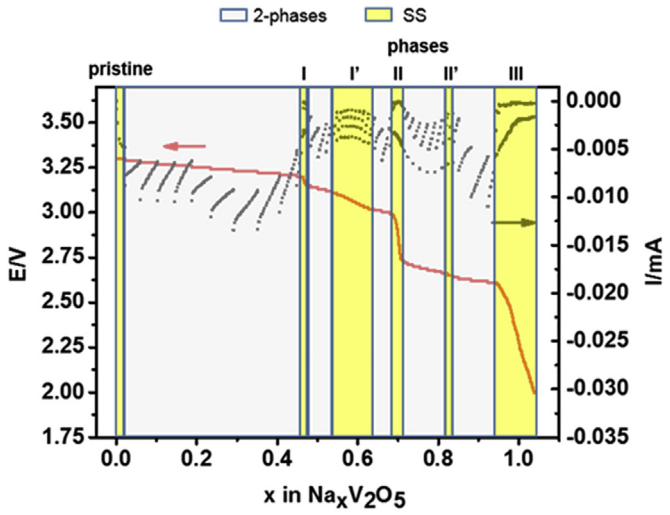

Fig. 6. Voltage/current vs. composition curves of a Na || HP-β-V_2O_5 cell run under potentiostatic intermittent conditions (10 mV/8 h). Solid solutions and two-phase regions are shaded in yellow and gray, respectively. (For interpretation of the references to colour in this figure legend, the reader is referred to the Web version of this article.)

In view of the complex voltage-composition profile shown in Figs. 2a and 5, which points to numerous structural phase transformations, potentiostatic intermittent titration technique (PITT; see experimental section) was used to shed more light on the high-voltage region of the Na || HP-β-V_2O_5 system regarding both compositional range of phases formed upon Na^+ insertion and their structures. Fig. 6 shows both the variation of current and voltage with sodium content in $Na_xV_2O_5$. On one hand, current relaxation in the gray shaded regions is far from a $t^{-1/2}$ power law and exhibit non symmetrical behaviour on both sides of $|I|$ maxima as exemplified in Fig. S4 a) and b) of Supporting Information. Such behaviour is related to regions where two phases coexist with varying relative ratio as x increases. On the other hand, current relaxes faster towards I = 0 in the yellow shaded regions, following a power law closer to $t^{-1/2}$ as exemplified in Fig. S4 c) and d) of Supporting Information. This is indicative of the formation of solid solutions.

The assignment of compositional regions made in Fig. 6 agrees with the interpretation of the GITT experiment (Fig. 5), since different current relaxation regimes can be observed. However, results from PITT and time dependence of current suggest the existence of another single phase (I') between phases I and II, separated from I and II by two narrow biphasic regions. An identical situation is found for another single phase, II', detected between phases II and III. Regarding phases I, II and III, we notice that compositional ranges deduced from both PITT and GITT only slightly differ despite their different experimental conditions. To summarize, the combination of PITT and GITT experiments evidences the existence of the following phases and compositional ranges:

Phase I: x = 0.35–0.45

Phase I': x = 0.55–0.65

Phase II: x = 0.65–0.7

Phase II': x = 0.83

Phase III: x = 0.9–1.0

In order to reveal the structural features of sodium storage during the electrochemical sodium insertion in HP-β-V_2O_5, ex-situ XRD was carried out. HP-β-V_2O_5 electrodes were discharged under constant current to different x values in the $0 \leq x \leq 1$ compositional range and investigated by X-ray diffraction. Particularly, four points were investigated in the discharge process of the first cycle, which correspond to the single-phase regions deduced from our GITT experiment. These are: before discharge (x = 0), discharging to 59 mAh g^{-1} at 3.13 V (corresponding to phase I, 0.4 Na), discharging to 103 mAh g^{-1} at 2.75 V (corresponding to phase II, 0.7 Na insertion), discharging to 132 mAh g^{-1} at 2.10 V (corresponding to phase III, 0.95 Na insertion).

Refined cell parameters of all above mentioned $Na_xV_2O_5$ compositions obtained by electrochemical discharge are summarized in Table 1. Selected 2θ angular regions together with the voltage composition curve are plotted in Fig. 7. For phase I (x = 0.4 Na), a significant shift of characteristic peaks, such as (100) and (−101) towards lower diffraction angles is observed, indicating an elongation of *a* parameter, and consequently, the separation of the V−O octahedral layers. $Na_{0.4}V_2O_5$ could be successfully indexed in the monoclinic system with a = 10.120(1) Å, b = 3.6073(3) Å, c = 6.3805(5)Å and β = 94.405(7)°. The XRD pattern of phase II (x = 0.7 Na) is similar to that of phase I exhibiting less pronounced shifts of (100) and (−101) peaks. Refined cell parameters for $Na_{0.7}V_2O_5$ are a = 10.097(1) Å, b = 3.6370(5) Å, c = 6.4187(4) Å and β = 92.992(8)°. For phase III (x = 0.95 Na), increase of intensity of (200) peak and decrease of intensity of (100) and (−101) become obvious. Indexing yielded the following cell parameters a = 9.576(1) Å, b = 3.5840(7) Å, c = 6.3171(8) Å and 92.91(1)°. The XRD pattern at the final charge state of the first cycle resembles the sodium intercalated compound rather than pristine non-intercalated HP-β-V_2O_5. Our interpretation is that, although a reversible Na insertion is inferred from electrochemical discharge-charge cycles, an irreversible transformation of V−O layers is likely produced after insertion of the very first Na^+ ions.

Interestingly, lithium insertion in α-V_2O_5 below 1.9 V has been reported to produce a new phase, ω-$Li_xV_2O_5$ (x = 3), that can be afterwards deintercalated and which is topotactically related to the α polymorph [26]. For sodium insertion in HP-β-V_2O_5 the structural

Table 1
Crystallographic data for selected compounds of the β-$Na_xV_2O_5$ system.

Phases	a/Å	b/Å	c/Å	β/°	Vol/Å^3
β-V_2O_5	7.1170(9)	3.5765(6)	6.2989(9)	90.09(1)	160.12(4)
$Na_{0.4}V_2O_5$	10.120(1)	3.6073(3)	6.3805(5)	94.405(7)	232.24(3)
$Na_{0.7}V_2O_5$	10.097(1)	3.6370(5)	6.4187(4)	92.992(8)	235.41(5)
$Na_{0.9}V_2O_5$	9.576(1)	3.5840(7)	6.3171(8)	92.91(1)	216.53(5)
De-$Na_{0.4}V_2O_5$	10.152(1)	3.6145(5)	6.3925(8)	94.17(1)	233.17(6)
De-$Na_{0.7}V_2O_5$	10.120(1)	3.6112(6)	6.3848(8)	94.28(1)	232.94(9)
De-$Na_{0.95}V_2O_5$	10.130(1)	3.5996(5)	6.3294(7)	94.38(1)	230.16(5)

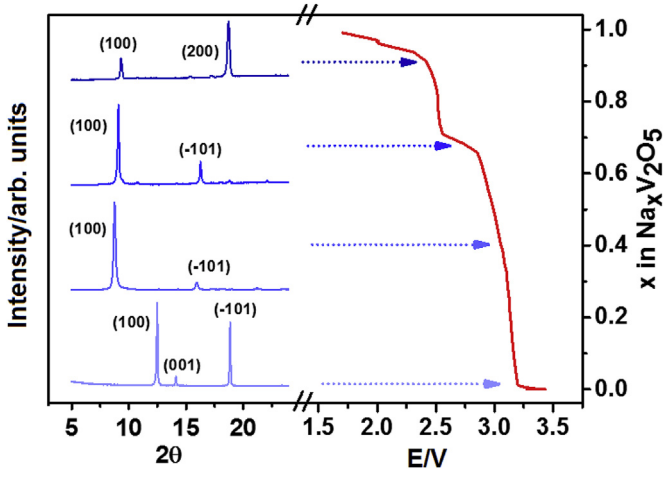

Fig. 7. Ex-situ XRD patterns of the $Na_xV_2O_5$ electrode obtained during the first discharge of high pressure β-V_2O_5 for selected compositions x = 0, 0.4, 0.7 and 0.9.

transformation is likely to occur at the very beginning of insertion reaction owing to the much bigger size of sodium ions.

In any case, a deeper insight into the structural changes and related phase transformations requires the use of high-resolution diffraction techniques such as synchrotron X-ray or neutron powder diffraction, under operando conditions if possible.

In order to prove the origin of the irreversible transformation, HP-β-V_2O_5 || Na cells were subjected to a complete discharge-charge cycle in which the amount of sodium was fixed to x = 0.4 (phase I), x = 0.7 (phase II) and x = 0.95 (phase III). The sodium deintercalated electrodes were then subjected to XRD post-mortem studies. Fig. 8 shows the discharge-charge cycles to x = 0.4 (a), 0.7 (b) and 0.95 (c) together with their respective ex situ XRD patterns. Most notably, the desodiated compounds exhibit rather similar XRD pattern, regardless of the amount of previously intercalated sodium, but quite different from that of HP-β-V_2O_5 (Fig. 8d). Accordingly, as it can be seen in Table 1, refined lattice parameters of all desodiated materials (De-$Na_xV_2O_5$) are similar to each other, but clearly different from those of HP-β-V_2O_5. We conclude from these findings that i) an irreversible structural transformation occurs upon the very first intercalated Na^+ being completed for x = 0.4 Na (phase I); ii) as a logical sequence deduced from X-ray pattern analysis of all desodiated phases, the structural transformations for x > 0.4 including the formation of phases II and III proceed reversibly. On the other hand, post-mortem analysis of an electrode cycled 150 times shows that the active material is still crystalline and exhibits the characteristic X-ray diffraction pattern of Phase I (see Fig. S5 of Supporting Information). To summarize, insertion of the very first sodium produces the transformation of HP-β-V_2O_5 to Phase I, $Na_{0.4}V_2O_5$, which further cycles. The good capacity retention upon long cycling (Fig. 2) can be attributed to the small volume change experienced by this material during sodium storage between Phase I and Phase III (NaV_2O_5).

We must recall now that Phase I exhibits less kinetic limitations than HP-β-V_2O_5 as deduced from the lower value of charge-transfer resistance determined by impedance spectroscopy (see above). Thus, the electrochemically driven phase transformation facilitates accommodation of sodium ions in more accessible sites, from which easy sodium extraction and inserted is favoured.

A comprehensive structural determination of the sodiated phases is currently under progress by mean of neutron powder diffraction combined with transmission electron microscopy and in operando synchrotron X-ray diffraction to draw a complete picture of the sodium intercalation path in HP-β-V_2O_5. Results will be published elsewhere.

4. Conclusions

In conclusion, we show for the first time a new sodium insertion material, high pressure β-V_2O_5, enabling up to 1 Na^+/V_2O_5 with a maximum discharge capacity of 147 mAh g^{-1} in the 3.6–2.0 V range. HP-β-V_2O_5 delivers a very attractive specific energy of 410 Wh kg^{-1} for cathode applications in sodium-ion batteries.

We demonstrate that the layered structure of HP-β-V_2O_5 favours the incorporation and mobility of Na^+ ions. Though high-pressure materials feel to be something away from large-scale application, the appealing electrochemical properties of HP-β-V_2O_5 unveiled in this work may trigger new advances in synthesis to make it easily available, like in the case of vanadium oxyfluoride VO_2F [4]. The high capacity exhibited by this oxyfluoride boosted the initiative of finding a more easily scalable preparation method based on high-energy ball-milling.

The structural study of sodiated materials confirms that an irreversible phase transformation occurs upon insertion of the very first sodium ions, however the insertion reaction proceeds topotactically in the whole compositional range investigated in this work. Interestingly,

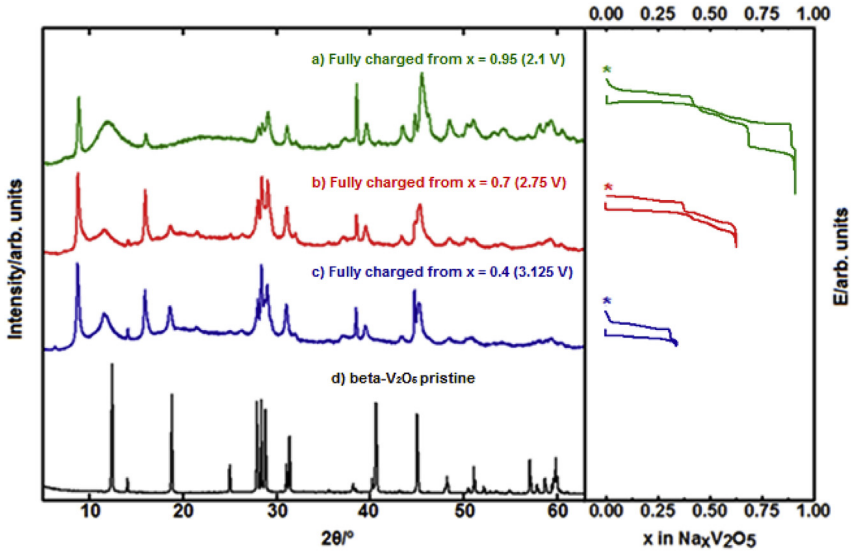

Fig. 8. Full discharge-charge cycles (right) and post mortem X-ray diffraction patterns (left) of HP-β-V_2O_5/Na cells at a C/20 rate. The amount of sodium was fixed to x = 0.4 in the 3.3–3.13 V range (a), to x = 0.7 in the 3.30–2.75 V range (b) and to x = 0.95 in the 3.30–2.10 V range (c).

the phase transformation improves electrochemical performance since charge-transfer resistance decreases.

Finally, we must notice that the amount of inserted sodium points to the reduction of only half of the available V^{5+} ions. Investigations suggestive of 2 e^- transfer for β-V_2O_5, which would lead to a high theoretical capacity of 300 mAh g^{-1}, are now under progress and will be published elsewhere.

CRediT authorship contribution statement

Rafael Córdoba: Investigation, Writing - original draft, Visualization. **Alois Kuhn:** Investigation, Conceptualization, Methodology, Writing - original draft, Writing - review & editing, Supervision. **Juan Carlos Pérez-Flores:** Investigation. **Emilio Morán:** Conceptualization. **José Manuel Gallardo-Amores:** Investigation. **Flaviano García-Alvarado:** Conceptualization, Methodology, Writing - original draft, Writing - review & editing, Supervision, Funding acquisition.

Acknowledgements

We thank Agencia Estatal de Investigación (AEI)/Fondo Europeo de Desarrollo Regional (FEDER/EU) and Comunidad de Madrid for funding the projects MAT2016-78632-C4-1, 4 -R and S2013/MIT-2753, respectively. R. Córdoba wants to thank AEI and FEDER/EU for the predoctoral grant BES-2017-080862.

Appendix A. Supplementary data

Supplementary data to this article can be found online at https://doi.org/10.1016/j.jpowsour.2019.03.018.

References

[1] V. Palomares, P. Serras, I. Villaluenga, K.B. Hueso, J. Carretero-Gonzalez, T. Rojo, Energy Environ. Sci. 5 (2012) 5884–5901.
[2] S.W. Kim, D.H. Seo, X.H. Ma, G. Ceder, K. Kang, Adv. Energy Mater. 2 (2012) 710–721.
[3] R.Y. Chen, S.H. Ren, M. Yavuz, A.A. Guda, V. Shapovalov, R. Witter, M. Fichtner, H. Hahn, Phys. Chem. Chem. Phys. 17 (2015) 17288–17295.
[4] J.C. Perez-Flores, R. Villamor, D. Avila-Brande, J.M.G. Amores, E. Moran, A. Kuhn, F. Garcia-Alvarado, J. Mater. Chem. 3 (2015) 20508–20515.
[5] M.A. Cambaz, B.P. Vinayan, O. Clemens, A.R. Munnangi, V.S.K. Chakravadhanula, C. Kubel, M. Fichtner, Inorg. Chem. 55 (2016) 3789–3796.
[6] C. Delmas, H. Cognacauradou, J.M. Cocciantelli, M. Menetrier, J.P. Doumerc, Solid State Ionics 69 (1994) 257–264.
[7] V.P. Filonenko, M. Sundberg, P.E. Werner, I.P. Zibrov, Acta Crystallogr. Sect. B Struct. Sci. 60 (2004) 375–381.
[8] M. de Dompablo, J.M. Gallardo-Amores, U. Amador, E. Moran, Electrochem. Commun. 9 (2007) 1305–1310.
[9] W.H. Baur, Am. Mineral. 57 (1972) 709.
[10] A.F. Reid, A.E. Ringwood, J. Solid State Chem. 1 (1970) 557–565.
[11] O. Garcia-Moreno, M. Alvarez-Vega, F. Garcia-Alvarado, J. Garcia-Jaca, J.M. Gallardo-Amores, M.L. Sanjuan, U. Amador, Chem. Mater. 13 (2001) 1570–1576.
[12] V. Raju, J. Rains, C. Gates, W. Luo, X. Wang, W.F. Stickle, G.D. Stucky, X. Ji, Nano Lett. 14 (2014) 4119–4124.
[13] Y. Lee, S.M. Oh, B. Park, B.U. Ye, N.-S. Lee, J.M. Baik, S.-J. Hwang, M.H. Kim, CrystEngComm 19 (2017) 5028–5037.
[14] G. Ali, J.H. Lee, S.H. Oh, B.W. Cho, K.W. Nam, K.Y. Chung, ACS Appl. Mater. Interfaces 8 (2016) 6032–6039.
[15] K. West, B. Zachauchristiansen, T. Jacobsen, S. Skaarup, Electrochim. Acta 38 (1993) 1215–1220.
[16] V.V. Kulish, S. Manzhos, RSC Adv. 7 (2017) 18643–18649.
[17] V.L. Volkov, B.G. Golovkin, A.S. Fedyukov, Y.G. Zainulin, Inorg. Mater. 24 (1988) 1568–1571.
[18] Q. Su, W. Lan, Y.Y. Wang, X.Q. Liu, Appl. Surf. Sci. 255 (2009) 4177–4179.
[19] A. Talledo, H. Valdivia, C. Benndorf, J. Vac. Sci. Technol. 21 (2003) 1494–1499.
[20] C.W. Zou, X.D. Yan, J. Han, R.Q. Chen, W. Gao, J. Phys. D Appl. Phys. 42 (2009).
[21] C.W. Zou, X.D. Yan, D.A. Patterson, E.A.C. Emanuelsson, J.M. Bian, W. Gao, CrystEngComm 12 (2010) 691–693.
[22] A.D. Wadsley, Acta Crystallogr. 8 (1955) 695–701.
[23] D. Su, G. Wang, ACS Nano 7 (2013) 11218–11226.
[24] D.W. Su, S.X. Dou, G.X. Wang, J. Mater. Chem. 2 (2014) 11185–11194.
[25] S. Tepavcevic, H. Xiong, V.R. Stamenkovic, X. Zuo, M. Balasubramanian, V.B. Prakapenka, C.S. Johnson, T. Rajh, ACS Nano 6 (2012) 530–538.
[26] C. Delmas, S. Brethes, M. Menetrier, J. Power Sources 34 (1991) 113–118.